Journal of Photochemistry and Photobiology 16 (2023) 100191

Contents lists available at ScienceDirect

Journal of Photochemistry and Photobiology

journal homepage: www.sciencedirect.com/journal/journal-of-photochemistry-and-photobiology

Peptide-bridged bis-porphyrin compounds: A photophysical and molecular dynamics study

Rita Cimino [a], Emanuela Gatto [a], Marta De Zotti [b,c], Fernando Formaggio [b], Claudio Toniolo [b], Micaela Giannetti [a], Antonio Palleschi [a], Carlos Serpa [d], Mariano Venanzi [a,*]

[a] Department of Chemical Science and Technology, University of Rome Tor Vergata, 00133, Rome, Italy
[b] Department of Chemistry, University of Padua, 35131, Padua, Italy
[c] Centro Interdipartimentale di Ricerca "Centro Studi di Economia e Tecnica dell'Energia Giorgio Levi Cases", 35131, Padua, Italy
[d] Chemistry Department, University of Coimbra, 3004-535, Coimbra, Portugal

ARTICLE INFO

Keywords:
Bis-porphyrins
Exciton coupling
Peptide spacers
Singlet oxygen production
Time-resolved spectroscopy
Ultrafast transient absorption

ABSTRACT

Covalently linked peptide-porphyrin compounds are most suitable systems for fundamental studies aiming to the comprehension of the mechanisms driving photoinduced energy/electron transfer processes. Mimicking photosynthetic units, the porphyrin groups act as antenna moieties while the peptide chain is the active medium through which energy and/or electron funneling occur. In this contribution we studied the transfer of excitation between two identical tetraphenylporphyrin groups connected by short peptide chains of different length formed by non-coded conformationally constrained α-amino acids, *i.e.*, C^{α}-methylvaline. The photophysical events following porphyrin photoexcitation were characterized from the microsecond to the picosecond time region by time-resolved spectroscopy techniques. Ultrafast transient absorption measurements revealed the presence of a transient species that we assign to a self-trapped exciton migrating through the peptide chain. The exciton species propagates the electronic coupling between the two porphyrin groups giving rise to a characteristic bisignate band measured by circular dichroism experiments. Molecular dynamics simulations strongly suggest that the long lifetime (hundreds of picoseconds) of the exciton species is determined by the rigidity of the C^{α}-methylvaline residues, that inhibited energy relaxation pathways coupled to torsional motions of the peptide chain.

1. Introduction

Porphyrins feature unique photophysical and photochemical properties, which foster application in a wide range of fields, spanning from biomedicine to molecular electronics [1,2]. Their very high extinction coefficients in the visible and near-IR regions, photoinduced electron-transfer efficiency, semiconducting capabilities, and moderate, but useful fluorescence quantum yields have been stimulating the development of porphyrin-based materials as photosensitizers in photodynamic therapy (PDT) [3] and dye sensitized solar cells [4]. Moreover, porphyrins demonstrate versatile building blocks in the construction of multicomponent architectures because of well-established and affordable synthetic procedures, high stability, and remarkable self-assembly properties [5].

When porphyrin sensitizers are excited to high-energy singlet states, they efficiently populate triplet states by intersystem crossing, generating radical oxygen species (ROS) by energy (EnT) and electron (ElT) transfer processes to molecular oxygen [6]. Photosensitizers usually produce superoxide anions, hydroxyl radicals and peroxides through a first ElT step, that triggers the apoptosis of cancer cells by further electron- or hydrogen-transfer reactions [7]. Alternatively, EnT from the photosensitizer to $^3O_2$ can generate singlet oxygen, which is the tissue-damaging species [8].

Among the highly populated family of porphyrin-based materials, *bis*-porphyrins have been used as core components for sensor devices capable of chiral recognition [9] and EnT/ElT donor(D)-acceptor (A) systems [10]. A variety of *bis*-porphyrin compounds have been synthesized in which porphyrin groups are connected by covalently linked spacers, characterized by flexible [11] or constrained [12] geometries. Free-base/free-base, free-base/metal or metal/metal porphyrins fused at the β,β'-positions [13], or bridged by a polyphenylene linker [14], a ferrocene group [15] or a 3_{10}- helical peptide [16,17] have been investigated as covalently linked homodimers in EnT/ ElT studies, aiming to develop hybrid devices mimicking natural photosynthesis. It

* Corresponding author.
E-mail address: venanzi@uniroma2.it (M. Venanzi).

https://doi.org/10.1016/j.jpap.2023.100191

Available online 13 June 2023

has been shown that in *bis*-porphyrins linked by conductive or *semi*--conductive bridges, the rate of singlet/singlet and singlet/triplet EnT increases under resonance condition, *i.e.* as the energies of the bridge singlet and triplet excited states approach that of the donor excited state [18].

EnT can occur at short distances through the Dexter exchange mechanism that requires the overlap of the D-A electronic distributions. Otherwise, long-range EnT can be described as a dipole-dipole process (Förster mechanism), the efficiency of which depends on the inverse of the sixth power of the distance, but also contains a relevant orientation factor [19,20]. In an array of porphyrin moieties, the energy can migrate within the array, mimicking the behavior of porphyrin antennas in photosynthetic units [21]. Gros et al. [22] studied singlet-singlet energy transfer for co-facial Zn-porphyrin (D) and *etio*-porphyrin (A) heterodimers, linked alternatively by a rigid or a flexible bulky spacer, showing how the structural and dynamical properties of the spacer can affect the EnT efficiency in these systems.

In the case of a rigid spacer (S), the D-A distance is the predominant factor controlling the ElT rate, so that ElT in D-S-A generally takes place by a through-space mechanism when the D-A pair is separated by small interchromophoric distances, *i.e.,* less than 20 Å, or via through-bond for distances up to 20–100 Å [23]. In bioinspired D-S-A systems mimicking photosynthesis, long-range ElT has been shown to occur through a series of redox steps involving the peptide bonds of the protein matrix [24]. Two mechanisms have been proposed to explain the efficiency of long-range ElT through peptide chains: the super-exchange mechanism, where electron tunneling occurs without transient occupation of the bridging states, and the hopping mechanism, where the amide bonds are involved in the process as transient residence sites [25].

The capacity of oligo- and polypeptide to transfer electrons over long distances have extensively been studied by time-resolved fluorescence and pump-probe transient absorption spectroscopies [26]. It has been pointed out that the peptide bridge does not act as a simple spacer separating the D-A pair, but it plays an active role favoring ElT over long distances, this property being most evident when a peptide spacer attains an α- or 3_{10}- helical conformation [27]. The unique ElT efficiency through helical peptide chains is explained by the ordered coupling of intramolecularly hydrogen-bonded (HB) amide sites, which mediate the travel of electrons or holes through the peptide chain [28].

As conformationally constrained α-amino acids show a high propensity to form helical structures, oligopeptides formed by C^{α}-tetrasubstituted α-amino acids have been largely used in supramolecular chemistry as templates or rigid spacers [29]. In C^{α}-tetrasubstituted α-amino acids, the C^{α} -H atom is substituted with an alkyl group, causing a severe restriction of the conformational energy region accessible to the φ and ψ torsional angles [30]. In particular, (L)-C^{α}-methylvaline [(αMe)Val] has been shown, by photophysical, NMR and theoretical conformational studies, to be one of the most efficient C^{α}-tetrasubstituted residues in the formation of rigid chiral peptide chains, attaining preferentially a 3_{10}-helix conformation [31–33]. The latter conformation is characterized by an $i \leftarrow i+3$ C = O•••H—N HB pattern, 3.34 number of residues per turn, a 6.29 Å helix pitch, 10 atoms involved in the formation of a single intramolecular H-bond, and φ=−63°and ψ=−42° torsional angles. Therefore, a 3_{10}–helix is tighter, more elongated, and slightly less stable than the α-helix, because of some HB distortion and unfavorable van der Waals interactions [34].

Herein, the photophysical properties of three *bis*-porphyrin peptide compounds comprising two identical tetraphenylporphyrin (TPP) units separated by [L-(αMe)Val] spacers of different length are presented, spanning a temporal range from the μs to the ps region. In the following, the investigated compounds of general formula TPP-CO-L-Ala-[L-(αM*e*)V*al*]$_n$-NH-cHe-NH—CO-TPP (n = 2, 4, 6) will be denoted by the acronym PMV*n*P, with n = 2, 4, 6 (Scheme 1).

The two TPP groups in the PMV*n*P compounds have already been shown to be coupled through exciton interaction by circular dichroism (CD) measurements [16]. Mark of the exciton interaction was the observation of an intense bisignate CD curve showing a positive maximum at 422 nm and a negative maximum at 413 nm, with a cross-over point at 417 nm in the proximity of the Soret absorption maximum. This effect was explained in terms of a (weak) long-range dipole-dipole interaction, excluding overlap of electronic distributions of the porphyrin pair [17]. It was found that TPP-TPP exciton coupling strongly depends on the relative distance and orientation of the two chromophores, and that it was still detectable over distances of about 30 Å. The intensities of the signals in terms of molar ellipticities were found to be PMV2P ($\Delta\varepsilon_{422}\approx+17$; $\Delta\varepsilon_{413}\approx-12$) >PBMV4P ($\Delta\varepsilon_{422}\approx+13$; $\Delta\varepsilon_{413}\approx-6$) >>PMV6P ($\Delta\varepsilon_{422}\approx+1$; $\Delta\varepsilon_{413}\approx+3$) [17]. Notably, the exciton-coupled CD is absent for PMV6P, where only two positive and weak Cotton effects could be detected. FTIR and NMR spectroscopy data indicated that all the PMV*n*P compounds attained a restricted conformational landscape [16,17].

Aim of this study is to determine the dependence of the *bis*-porphyrin exciton-coupling interaction, well established by CD spectroscopy measurements, on the structural and dynamical properties of the peptide bridge. The nature of the exciton-coupling interaction between the two porphyrin moieties was investigated by fluorescence and transient absorption time-resolved experiments. Molecular Dynamics (MD) simulations have also been carried out to obtain information on the dynamical properties of the peptide chain bridging the two porphyrin moieties. The reported results are expected to open new perspectives in the design of porphyrin-based photosensitizers to be used in PDT of tumors or as photoactive elements in Dye-Sensitized Solar Cells (DSSC's).

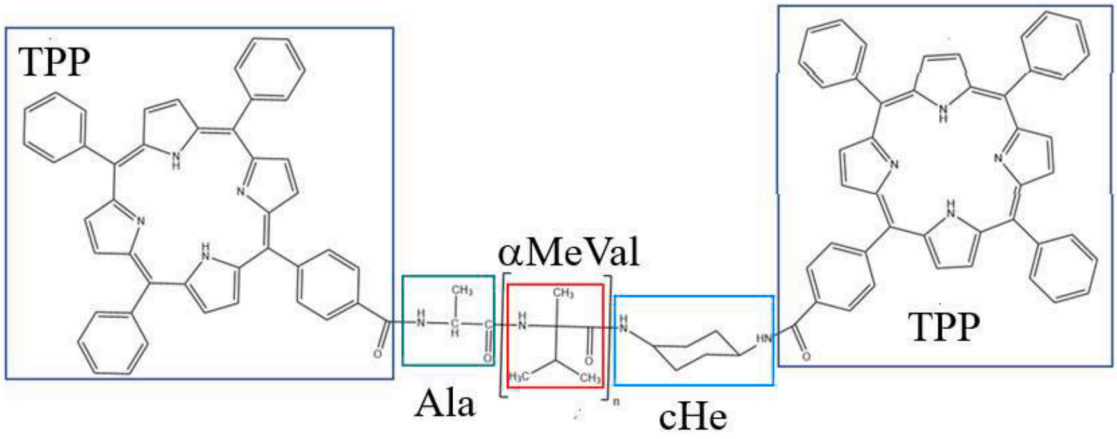

Scheme 1. Chemical structure of the bis-porphyrin-compounds investigated. Acronym PMVnP: n = 2,4,6. The alanine (Ala) and cyclohexane (cHe) groups linking the TPP moieties to the α(Me)Val-oligopeptide chain are also shown.

2. Experimental section

2.1. Chemicals

The synthesis and characterization of the peptide-bridged *bis*-porphyrin compounds here investigated were already reported elsewhere [16]. TPP was kindly supplied by Carlos Monteiro (Luzitin). Solvents such as acetonitrile (99.9%), toluene (99,8%), methanol (99.9%) and glycerol (99.5%) were purchased from Fisher. Perinaphthenone (1H-phenalen-1-one) (97%), purchased from Sigma Aldrich, was used as photosensitizer for the determination of singlet oxygen quantum yield. All the solvents and chemical reagents were used as received. All spectroscopic experiments were carried out using quartz cuvettes of 1-cm optical path (l) with exception of femtosecond transient absorption measurements ($l = 0.2$ cm).

2.2. Methods

2.2.1. UV/Vis absorption spectra

Absorption spectra in solution were recorded with a Shimadzu UV-2100 (Japan) spectrophotometer and recorded from 350 to 700 nm.

2.2.2. Fluorescence spectroscopy

Steady-state fluorescence spectra were carried out on a Horiba-Jobin-Ivon SPEX Fluorolog 3–22 spectrophotometer, setting excitation and emission slit- widths at 2.5 nm. Samples were excited at λ_{ex}=414 nm and the emission spectra were collected from 600 to 800 nm. Relative fluorescence quantum yields (Φ_f) of PMV*n*P were determined with respect to the TPP reference compound upon excitation at λ_{ex}=511 nm in toluene (Φ_f^R=0.11) [35], using Eq. (1):

$$\Phi_f = \Phi_f^R \frac{I_f}{I_f^R} \frac{A^R}{A} \left(\frac{n}{n^R}\right)^2 \quad (1)$$

where the superscript "R" indicates the reference compound, Φ_f the fluorescence quantum yield, I_f the integrated fluorescence intensity, A the absorbance at the excitation wavelength and n the refractive index of the solvent used [n(toluene) = 1.49693; n(acetonitrile) = 1.3404]. The *bis*-porphyrins and reference compounds were excited at λ_{ex} = 511 nm. All the solutions were degassed for 20 min by fluxing ultrapure nitrogen, unless otherwise stated.

Fluorescence decays were measured using a home-built, time-correlated single photon counting (TCSPC) apparatus equipped with a Horiba-Jobin-Yvon Nanoled excitation source (λ_{ex}= 373 nm, IRF_{FWHM}~ 1 ns). Emission was collected at 90° geometry through a double subtractive Oriel Cornerstone 260 monochromator and detected by a Hamamatsu microchannel plate photomultiplier (R3809U-50). Signal acquisition and data processing were performed employing a Becker&Hickl SPC-630 TCSPC module.

Fluorescence time decays and the instrumental response function (IRF) were collected over 1024 channels (100 ns time window), until 5 × 10^3 counts at maximum were reached. Deconvolution of the fluorescence decay curves was performed using the modulating function method as implemented in the SAND program [36]. TPP and PMV2P decays were collected at λ_{em} = 655 nm, while for PMV4P and PMV6P the decays were collected at λ_{em} = 635, 660 and 710 nm. If necessary, the samples were accurately degassed to minimize oxygen quenching, and the optical densities of the *bis*-porphyrin and reference solutions were adjusted so that the absorbance at the excitation wavelength (λ_{ex}=373 nm) resulted to be around 0.2.

Anisotropy time decays were measured at λ_{ex}= 409 nm and λ_{em}= 650 nm at 292 K, applying Eq. (2):

$$r(t) = \frac{I(t)_{VV} - I(t)_{VH}}{I(t)_{VV} + 2 * I(t)_{VH}} \quad (2)$$

Where the time decay intensities at time t $I(t)_{VV}$ and $I(t)_{VH}$ were measured with a vertical excitation polarizer and a vertical and horizontal emission polarizer, respectively. Rotational correlation times, τ_r, were obtained by fitting the anisotropy decay, r(t), within the spherical rotor approximation, (Eq. (3)):

$$r(t) = r_0 exp(-t/\tau_r) \quad (3)$$

2.2.3. Nanosecond transient absorption

Time-resolved triplet-triplet absorption spectra and triplet state decays were recorded by an applied Photophysics LKS.60 laser flash photolysis spectrometer equipped with a Hewlett-Packard Infinium Oscilloscope and a Spectra-Physics Quanta-Ray GCR-130 Nd:YAG laser as the excitation source (E_{max} = 30 mJ per pulse, FWHM = 6 ns). At least seven kinetic runs for aerated and N_2–flushed acetonitrile freshly prepared solutions were acquired at room temperature for each sample. For all the experiments each solution was prepared with an absorbance of about 0.2 at the excitation wavelength. The same apparatus in emission mode and coupled to a NIR detector was used to measure the singlet oxygen sensitization quantum yield. Room temperature singlet oxygen phosphorescence at λ_{em}=1270 nm from aerated solutions of the samples was collected with a Hamamatsu R5509–42 photomultiplier cooled with liquid nitrogen at 193 K. The modifications to the spectrometer included the use of a Melles Griot (03MCS005) cold mirror and a Schott filter RG850 to cut the excitation scattered light and the samples emission harmonics. Both entrance and exit slits of the monochromator were set at 3 nm.

2.2.4. Ultrafast transient absorption

Ultrafast transient absorption experiments were carried out using a broadband (350–1600 nm) HELIOS pump-probe femtosecond transient absorption spectrometer from Ultrafast Systems. A Spectra-Physics Solstice-100F laser (128 fs pulse width; 1 kHz repetition rate) coupled with a Spectra-Physics TOPAS Prime F optical parametric amplifier (195–22,000 nm) was used for pulse pump generation. Probe light in the Vis (450–800 nm) and NIR (800–1600 nm) ranges was generated by passing a small portion of the 795 nm light from the Solstice-100F laser through a computerized optical delay (7.6-ns time window) and focusing it in a sapphire plate to generate a white-light continuum. All measurements were carried out in a 2-mm quartz cuvette with optical densities below 0.3 and using pump excitation energies below 0.5 mJ. To minimize photodegradation, the solutions were stirred during the experiments. Transient absorption data were analyzed using the Surface Xplorer PRO program from Ultrafast Systems.

2.2.5. Molecular dynamics simulations

MD simulations were performed using the AMBER99 force field as implemented in the GROMACS v. 5.1.2 software package [37]. The parameters used for TPP, cHe, and the (αMe)Val-moieties are reported as Supplementary Information (SI, Table T1). Parameters for TPP were obtained starting from the porphyrin parameters reported by Paulo et al. [38]. (αMe)Val-parameters were generated in analogy with those of the standard amino acids present in the AMBER force field. The parameters for acetonitrile (SI, Table T1) were optimized by reproducing the experimental density of the solvent [39].

Two MD simulations of 200 ns time length each have been performed for the three *bis*-porphyrin compounds. In the simulation cubic box (9.5 × 9.5 × 9.5 nm^3) a molecule of the investigated compound and 6084 solvent molecules were inserted, applying periodic boundary conditions in the XYZ directions. A cut-off approach was used for coulombic and van der Waals interactions using a potential-shift-Verlet modifier with a cut-off distance of 1.4 nm. Within the weak coupling regime, a temperature/velocity coupling rescaled with a time constant of 0.6 ps and a reference temperature of 300 K were used for the NPT simulation. No pressure coupling was applied. All the chemical bonds were constrained using the LINCS constraint-algorithm, except during the equilibration and annealing steps (time step of 0.5 fs). The compressibility was put

equal to $9.5{\cdot}10^{-6}$ bar^{-1}. Cluster analysis for the three systems investigated was carried out applying a cut-off of 0.13 nm and using the linkage method as implemented in GROMACS.

3. Results and discussion

3.1. Singlet state properties

Porphyrins feature a widely delocalized π-electron distribution causing strong absorption in a large region of the UV–Vis spectrum. All the PMV*n*P compounds, here investigated in acetonitrile, show the typical absorption spectrum of the porphyrin chromophore, presenting a sharp and very intense Soret band ($S_0 \rightarrow S_2$), peaked at λ_{max}=414 nm, and the less intense Q bands system ($S_0 \rightarrow S_1$) with absorption maxima at λ_{max}=511, 546, 589 and 645 nm (Supporting Information, Figure SI1). It should be noted that the ratio between the Soret transition and the first Q band oscillatory strengths is very sensitive to the aggregation state of the porphyrin compound. For TPP (reference compound), PMV2P, PMV4P and PBMV6P this ratio amounts to 26, 24, 25 and 22, respectively, which indicates that the investigated samples are predominantly in a non-aggregate state under the applied experimental conditions. As compared to TPP, a weak bathochromic shift ($\Delta\lambda \approx 1$ nm) of the Soret transition can be observed for all the PMV*n*P samples under investigation, most likely due to the covalent linkage of the porphyrin moieties to the peptide bridge.

Free-base porphyrins give also rise to significant fluorescence emission in the Vis region. The fluorescence emission spectra of the PMV*n*P compounds are quite similar to the emission of the TPP reference compound, characterized by a structured emission band peaked at λ_{em}=650 nm [Q(0,0)] and 715 nm [Q(0,1)] (Fig. 1). In the *bis*-porphyrin compounds a slight hypsochromic shift of the emission bands and a slight decrease of the Q(0,0)/Q(0,1) intensity ratio could be observed, pointing to a weak interaction between the porphyrin units or the porphyrin/peptide bridge (Table 1).

Interestingly, the fluorescence quantum yields of the PMV*n*P compounds in N_2-saturated solutions were found to slightly increase with respect to the TPP reference with the lengthening of the peptide bridge (Table 1).

Fluorescence lifetimes for PMV*n*P and TPP were measured in acetonitrile by the TCSPC method (Figs. 2 and SI2).

In general, the PMV*n*P decays are well fitted with a single exponential decay law with lifetimes of ~12 ns. The exception was PMV6P, where the decays are best fitted with a biexponential decay law (Figure SI2): a minor faster component τ_1 = 2.81 ns (α_1= 0.07) and a predominant slower component τ_2 = 12.1 ns (α_2=0.93), similar to the lifetime of the reference porphyrin compound.

Table 1
Spectroscopic (fluorescence λ_{max}, intensity ratio) and photophysical properties (fluorescence quantum yields, Φ_F, fluorescence lifetimes, τ_F, radiative, k_{rad} and radiationless rate constants, k_{nr}) for TPP and bis-porphyrin compounds (PMVnP, n = 2,4,6) in acetonitrile (T = 25 °C).

Samples	F[Q(0,0)]/ F[Q (0,1)]	Φ_f[a]	τ_f (ns)[b]	k_{rad} [*10^6 (s^{-1})]	k_{nr} [*10^7 (s^{-1})]
TPP	2.1	0.10	11.7	8.6	7.7
PMV2P	1.9	0.11	12.0	9.2	7.4
PMV4P	1.8	0.12	12.1	9.9	7.3
PMV6P	1.7	0.13	12.1	10.7	7.2

[a] N_2-saturated solution, using TPP in toluene as reference compound [33]. Error: ±0.01.
[b] Error: ±0.1 ns.

The short-time component may be tentatively assigned to a conformer in which the two porphyrin moieties interact each other, causing excited state fluorescence quenching. Radiative (k_r) and non-radiative (k_{nr}) decay rate constants of the PMV*n*P compounds, obtained by the experimental fluorescence quantum yields and time-decays (Eq. (4)), are reported in Table 1.

$$k_r = \frac{\phi_f}{\tau_f} k_{nr} = \frac{1}{\tau_f} - k_r = \frac{1}{\tau_f}\left(1 - \phi_f\right) \tag{4}$$

These results clearly indicate that the peptide spacer slightly affects the singlet state relaxation processes. In particular, the PMV*n*P compounds exhibit a marginal enhancement of fluorescence quantum yields and longer decay times as the length of the peptide spacer increases, giving rise to slightly increasing radiative rate constants and decreasing non-radiative rate constants for the longer homologues of the series.

Fluorescence anisotropy decay measurements were carried out to obtain information on the mobility of the samples under investigation (SI, Table T2). In methanol solutions, the fluorescence anisotropy of TPP and PMV*n*P decays with a single lifetime of about 300 ps, that can be associated to emission depolarization caused by the overall rotational motion of the fluorophores. Fluorescence anisotropy decay measurements carried out in a 70/30 methanol/glycerol solution (η=11 cPs) showed a significant decrease of the mobility of the molecules.

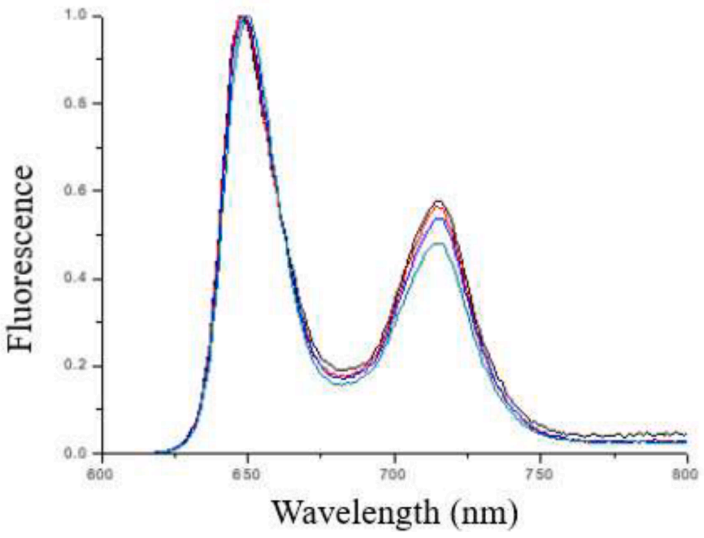

Fig. 1. Emission spectra of the samples in aerated acetonitrile measured upon excitation at 511 nm. Light blue: TPP; blue: PMV2P; red: PMV4P; black: PMV6P. The spectra were normalized to unity at λ=649 nm.

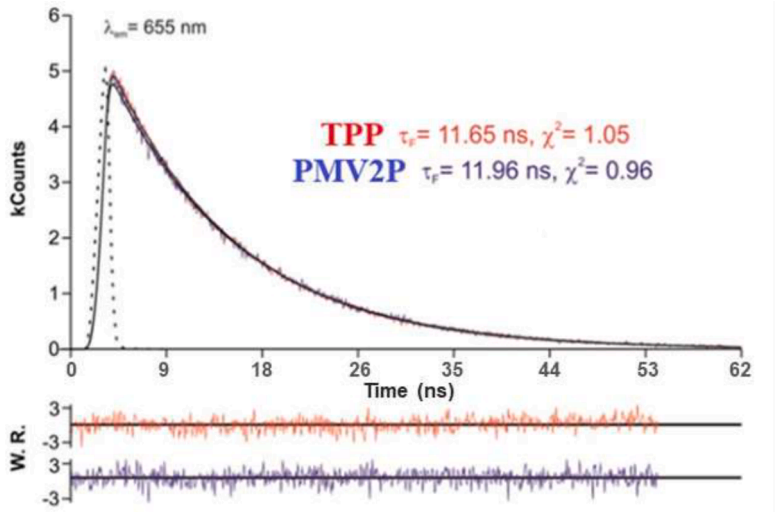

Fig. 2. Experimental and reconstructed time decays of TPP (red) and PMV2P (blue). The experimental excitation pulse is reported as a dashed line. The weighted residuals of the reconstructed *vs.* experimental decay are also reported. In the inset the lifetimes of TPP (red) and PMV2P (blue) obtained by the iterative deconvolution fitting procedure are shown.

Consequently, an increase of the overall rotational time of the *bis*-porphyrin compounds can be observed in the viscous medium with respect to TPP (230 ps). Interestingly, the rotational correlation time of PMV4P (1.02 ns) is significantly slower than those of PMV2P (640 ps) and PMV6P (590 ps), suggesting a higher conformational rigidity of the mid-term homologue of this series.

3.2. Triplet state properties

To further investigate the excited state dynamics of the PMV*n*P compounds time-resolved nanosecond transient absorption spectra (TAS) were measured with excitation at 355 nm, together with the singlet oxygen photosensitized quantum yields. The obtained singlet-triplet difference absorption spectra show a depletion band in the Soret region and a triplet state band centered at 450 nm, which are observed under both aerated and de-aerated solutions of all the samples under investigation. As an example, in Fig. 3 we illustrate the TAS's of PMV4P in N_2-saturated and in aerated acetonitrile solutions. The same results for TPP, PMV2P and PMV6P are reported as SI (Figures SI3-SI5).

The triplet lifetimes (τ_T) obtained by the best-fitting of the reported decay curves are listed in Table 2. All the samples showed comparable triplet-state lifetimes in aerated solutions, suggesting that oxygen-quenching processes predominate over all other competitive relaxation pathways involving the porphyrin triplet state. From the triplet-state lifetimes and the oxygen concentration in acetonitrile (9.1 mmol L^{-1}) [40], the triplet-state oxygen quenching rate constant results to be 3.0 ($\pm$0.1)·10^8 M^{-1} s^{-1} for the reference compound and all the *bis*-porphyrins investigated.

Table 2
Triplet-state lifetimes (τ_T), triplet-state (Φ_T) and singlet-oxygen (Φ_Δ) quantum yields of PMVnP and TPP (reference compound) in aerated and in N_2-saturated acetonitrile solutions.

	τ_T (TPP)	τ_T(PMV2P)	τ_T(PBMV4P)	τ_T(PMV6P)
aerated	353 ns	378 ns	376 ns	357 ns
N_2-flushed	28 μs	17 μs	34 μs	47 μs
	Φ_T (TPP)[a]	Φ_T(PMV2P)	Φ_T(PMV4P)	Φ_T(PMV6P)
aerated	0.88	0.58	0.79	0.73
	Φ_Δ(TPP)	Φ_Δ (PMV2P)	Φ_Δ (PMV4P)	Φ_Δ (PMV6P)
	0.61 ± 0.07	0.38 ± 0.06	0.34 ± 0.05	0.45 ± 0.07

[a] Triplet quantum yield used as reference in acetonitrile [38].

Interestingly, in de-aerated solutions, the triplet lifetime steadily increases with increasing the number of L-(αMe)Val-residues in the peptide chain, paralleling the photophysical behavior of the PMV*n*P's singlet state.

The triplet-state formation quantum yields, ϕ_T, were obtained by the singlet-depletion method (measuring transient decays at two different

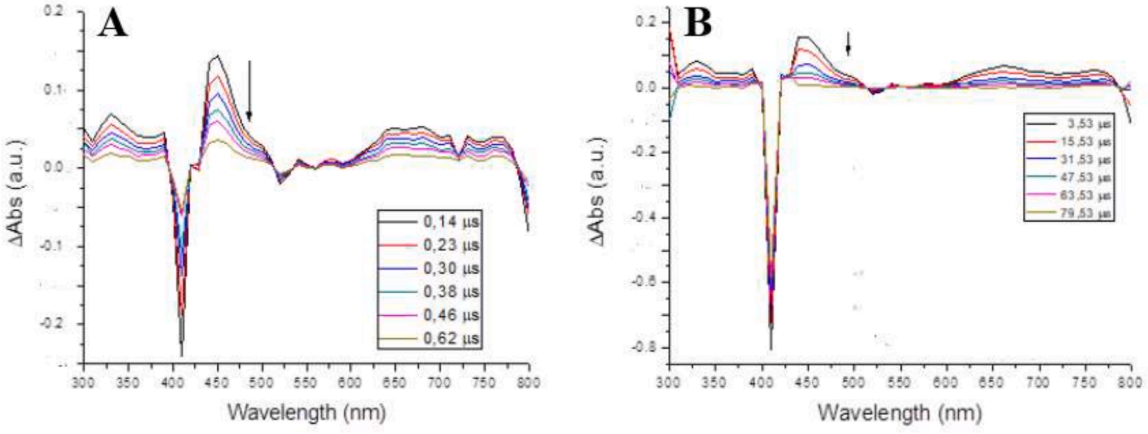

Fig. 3. Nanosecond transient absorption spectra of PMV4P in acetonitrile: A) aerated solution; B) N_2-saturated solution (λ_{ex}=355 nm).

wavelengths, *i.e.,* at λ=421 nm for the singlet depletion and λ=460 nm for the triplet absorption) (Table 2). From the exponential fit of these decays, the pre-exponential parameters, ΔOD_T and ΔOD_S, are employed to calculate the triplet molar absorption coefficient (ε_T) using the singlet-depletion method and the ground-state molar absorption coefficient (Eq. (5)). The triplet molar absorption coefficient and the pre-exponential factors from the triplet absorption were therefore used (Eq. (6)) to derive the triplet quantum yield (Φ_T) [41].

$$\epsilon_T = \frac{\epsilon_S \cdot \Delta OD_T}{\Delta OD_S} \tag{5}$$

$$\Phi_T = \frac{\epsilon_T^{ref} \cdot \Delta OD_T}{\epsilon_T \cdot \Delta OD_T^{ref}} \cdot \Phi_T^{ref} \tag{6}$$

The PMV*n*P samples under investigation present a lower triplet quantum yield with respect to that of the reference compound. Considering the sum of Φ_T and Φ_f, it can be argued that for PMV2P ($\Phi_T + \Phi_f = 0.71$), non-radiative processes significantly contribute to its relaxation pathway. For the longer compounds of the series, the importance of non-radiative processes decreases, being $\Phi_T + \Phi_f$ equal to 0.92 and 0.83 for PMV4P and PMV6P, respectively.

3.3. Singlet oxygen quantum yield

As the *bis*-porphyrin compounds investigated have a relatively long triplet lifetime, the oxygen quenching is very efficient, as shown by comparison of the PMV*n*P triplet lifetime measurements in aerated and de-aerated solutions (Table 2). Typically, porphyrins transfer a large part of their triplet-state energy to molecular oxygen, leading to high-yield production of singlet oxygen. Singlet-oxygen quantum yields (Φ_Δ) were obtained by measuring the phosphorescence decay of singlet oxygen ($^1O_2$*) at 1270 nm, following pulse laser excitation at λ_{ex}=355 nm of the TPP and PMV*n*P compounds. Perinaphthenone in acetonitrile, where singlet oxygen shows a long lifetime (77 μs) and a very high quantum yield (0.98), was used as reference compound [42]. Φ_Δ is obtained by extrapolating the measured luminescence intensities at zero time ($t = 0$) using Eq. (7) [43]:

$$\Phi_\Delta = \frac{L_\Delta(S)_{t=0}}{L_\Delta\left(S^{ref}\right)_{t=0}} \Phi_\Delta^{ref} \tag{7}$$

$L_\Delta(S)_{t=0}$ is obtained by the slope of the graph reporting the intensities of the phosphorescence decay curves as a function of the laser relative energy (Figures SI6, SI7). Singlet-oxygen quantum yields of the investigated compounds are reported in Table 2. The obtained TPP singlet-oxygen quantum yield is 0.61 in agreement with literature data [41].

From the triplet- and singlet-oxygen quantum yields, it is also possible to calculate the fraction of the porphyrin triplet state quenched by oxygen (f_Δ^T), which results to be 0.66, 0.43 and 0.62 for PMV2P, PMV4P and PMV6P respectively. Interestingly, the *bis*-porphyrin compounds presented lower singlet-oxygen quantum yield with respect to TPP, but comparable triplet/singlet oxygen quenching fraction [f_Δ^T(TPP) =0.69], except for PMV4P.

By bringing together the experimental results concerning triplet-state properties, it can be postulated that the *bis*-porphyrin compounds feature almost the same properties as the TPP reference: long triplet lifetime, and high triplet- and singlet-oxygen quantum yields. However, these values change by varying the length of the peptide chain bridging the two porphyrin groups. It was found that in de-aerated solutions, PMV6P shows a longer triplet lifetime whereas PMV2P a shorter one with respect to that of TPP, although the triplet-state quenching rate constant by oxygen is almost the same for all the samples and the reference. Interestingly, although PMV2P presents a lower triplet quantum yield than those of the other two compounds, it generates singlet oxygen with an efficiency of 66%, which is higher than the one produced by PMV4P (43%). Moreover, although PMV4P and PMV6P exhibit comparable triplet quantum yields, nevertheless PMV6P presents a sensibly higher singlet-oxygen quantum yield (61%). These findings are crucial for PDT applications of the PMV*n*P compounds.

3.4. Ultrafast transient absorption

Femtosecond TAS's and the associated decay kinetics for TPP and PMV*n*P compounds in acetonitrile, were collected with excitation at 535 nm in a 7.6-ns time window (Fig. 4 and Figure SI7).

The TPP TAS show several broad positive bands in the 450–800 nm spectral range, negative signals due to ground state depletion at λ= 512 and 647 nm, and two bleaching minima at λ= 548 and 590 nm corresponding to the porphyrin Q band system. For wavelengths higher than 700 nm a slowly growing component is clearly observed together with a depletion minimum at λ= 719 nm which is related to the porphyrin emission bands. PMV2P and PMV4P TAS spectra show essentially the same features (Figure SI8).

Baskin et al. [44] studied the ultrafast dynamics of TPP in benzene for different excitation wavelengths, spanning the whole absorption range from the B to the Q bands. Three distinct processes were found to affect the Q_x band relaxation: intramolecular vibrational relaxation (100–200 fs), relaxation by collision with the solvent (1.4 ps), and energy exchange with solvent until thermal equilibrium (10–20 ps). Analyzing the Q band relaxation of TPP at λ= 535 and 568 nm, a predominant slow component (τ_1~ 9 ns, α_1=0.90), comparable with the fluorescence lifetime, is ascribed to the decay of the relaxed Q_x state. A fast lifetime component (τ_2~ 2 ps, α_2=0.10) is assigned to solvent-induced vibrational relaxation [44]. These two decay time components were also found for all the PMV*n*P compounds with little changes, *i.e.* τ_1~ 10 ns (α_1=0.70) and τ_2~ 1 ps (α_2=0.10).

Moreover, the inclusion of a third decay time component of some hundred picoseconds was found to be necessary to fit adequately the PMV*n*P decay kinetics, but not for the TPP reference compound. Notably, this relatively slow time component is quite sensitive to the number of the (αMe)Val-residues in the peptide bridge, lasting τ_3=261, 453 and 241 ps at λ= 535 nm and τ_3= 191, 463 and 367 ps at λ= 568 nm for PMV2P, PMV4P and PMV6P, respectively (Table 3).

Interestingly, this third decay time component does not depend regularly on the length of the peptide bridge, *i.e.* it increases from $n = 2$ to $n = 4$ and then decreases for $n = 6$, suggesting an important role of the conformational and dynamical features of the peptide chain on the photophysical behavior of the investigated compounds.

The τ_3 decay time, too fast to be properly detected by nanosecond transient-absorption experiments, and not revealed by time-resolved fluorescence measurements, is too slow to be assigned to an intramolecular radiationless process. We are very tempted to ascribe this decay component to a trapped exciton species resulting from energy transfer between the porphyrin homodimers mediated by the peptide bridge [45]. This hypothesis is supported by the CD experiments reported by Guryanov et al. [17], showing that the two porphyrin chromophores are interacting through exciton coupling. The distinctive mark of this interaction is the typical bisignate chiral signal resulting from the induced Cotton effect exerted by the peptide bridge on the achiral TPP units. In the weak regime, this interaction can be described by a through-space (long-range) dipole-dipole interaction, highlighting the role of the conformational and dynamical properties of the peptide spacer bridging the two porphyrin moieties. In the specific case under investigation, these considerations are emphasized by the conformationally-constrained nature of the rigid $[(\alpha Me)Val]_n$ spacer.

3.5. Molecular dynamics simulations

The ultrafast TAA experiments described above demonstrate that, in the PMV*n*P compounds examined, the efficiency of exciton transfer and relaxation between the porphyrin groups depends on the conformational

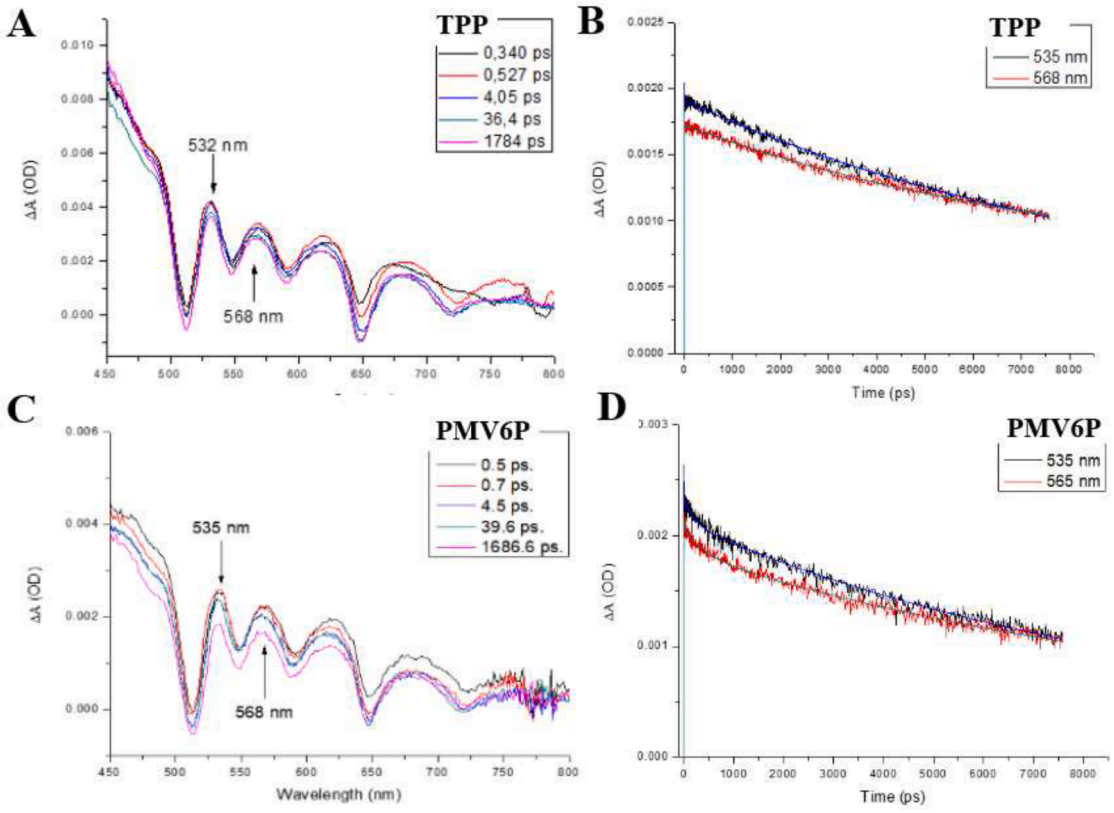

Fig. 4. Femtosecond transient absorption spectra of TPP (A) and PMV6P (C) in acetonitrile measured at different time decays after excitation at λ= 420 nm. The kinetic traces of TPP (B) and PMV6P (D) measured at λ= 535 (blue line) and 568 nm (red line) are also illustrated.

Table 3
Time decay parameters of the kinetic traces (λ= 535 and 568 nm) from the ultrafast transient absorption experiments on TPP and the bis-porphyrin compounds bridged by two (PMV2P), four (PMV4P), and six (PMV6P) α-amino acids.

	λ(nm)	τ_1 (ns)	τ_2 (ps)	τ_3 (ps)	α_1	α_2	α_3
TPP	535	9.5	1.9	–	0.9	0.1	–
	568	8.4	1.6	–	0.9	0.1	–
PMV2P	535	9.6	2.7	261.0	0.7	0.1	0.2
	568	10.3	0.5	191.1	0.7	0.1	0.2
PMV4P	535	10.0	0.9	453.3	0.7	0.2	0.1
	568	10.2	1.0	463.1	0.8	0.1	0.1
PMV6P	535	9.9	1.0	241.2	0.8	0.1	0.1
	568	10.8	0.8	367.0	0.8	0.1	0.1

properties of the peptide spacer.

Molecular Dynamics (MD) simulations were therefore carried out to obtain information on the structural (relative distance and orientation) and dynamical (peptide bridge and porphyrin-peptide linkages flexibility) properties of the two porphyrin groups in the PMV*n*P compounds. Examples of their most representative structures, as provided by cluster analysis of the corresponding 200 ns MD simulations, are shown in Fig. 5. The distance distribution between the centers of mass of the two porphyrin moieties in the PMV*n*P compounds are reported in Figure SI9.

In the case of PMV2P (Figs. 5A and SI9A) two main conformers were obtained, the more abundant (62.3%) presenting the two porphyrin moieties far apart (d = 27.4 ± 2.8 Å), and the second one (37.2%) showing the two groups quite closer, most likely stabilized by π-π stacking interactions (d = 6.1 ± 0.5 Å). Interestingly, PMV4P (Figs. 5B and SI9B) presents a single predominant conformation (99.3%), characterized by a TPP-TPP distance distribution peaked at 29.7 ± 2.7 Å. Cluster analysis of PMV6P, the longest term of the series, show two main conformations (Figs. 5C and SI9C) characterized by statistical weights of 74.6 and 21.5%, and TPP-TPP distances of 23.1 ± 1.5 Å and 32.6 ± 2.5 Å, respectively.

The MD simulation prediction of a compact conformation of PMV2P stabilized by π-π stacking of the porphyrin electronic distributions (Figure 8A) deserves a deeper insight. It should be noted that this conformation was not found for both PMV4P and PMV6P compounds. For this reason, we re-analyzed the PMV2P MD data and we extended the simulation time for this compound to 1 μs. The MD results were essentially confirmed, even if cluster analysis revealed that the weight of stacked porphyrin structures lowered to less than 20%. Spectroscopic experiments did not provide evidence of π-π interaction between the two porphyrin groups. If the lack of time resolved fluorescence evidence could be explained in terms of a non-fluorescent conformer, nevertheless, in this case, fluorescence quantum yields should have been affected by such interaction, and this was not observed. The only experimental evidence of a peculiar behavior of PMV2P is given by nanosecond transient absorption experiments, that showed a significantly lower triplet state population of PMV2P with respect to the other *bis*-porphyrin compounds investigated (Table 2). This finding suggests that, in the case of PMV2P, π-π stacking interaction does not affect the population of the excited singlet state, but rather inhibits singlet-to-triplet state crossing, promoting non-radiative relaxation pathways.

The flexibility of the oligopeptide spacer in PMV*n*P compounds can be best analyzed by taking into account the root mean-square fluctuation (RMSF) of the positions of all the amino acid residues and linkers at every picosecond of the MD trajectory. All the MD simulations show that the peptide spacer is quite rigid, especially in the $[L\text{-}(\alpha Me)Val]_n$ region (Fig. 6). In particular, PMV4P showed the highest rigidity of the bridge separating the two porphyrin groups. For this compound, in agreement with the results of cluster analysis, also the mobility of the two porphyrin end groups appears significantly reduced with respect to that of PMV2P and PMV6P. This effect is particularly relevant for Ala-and

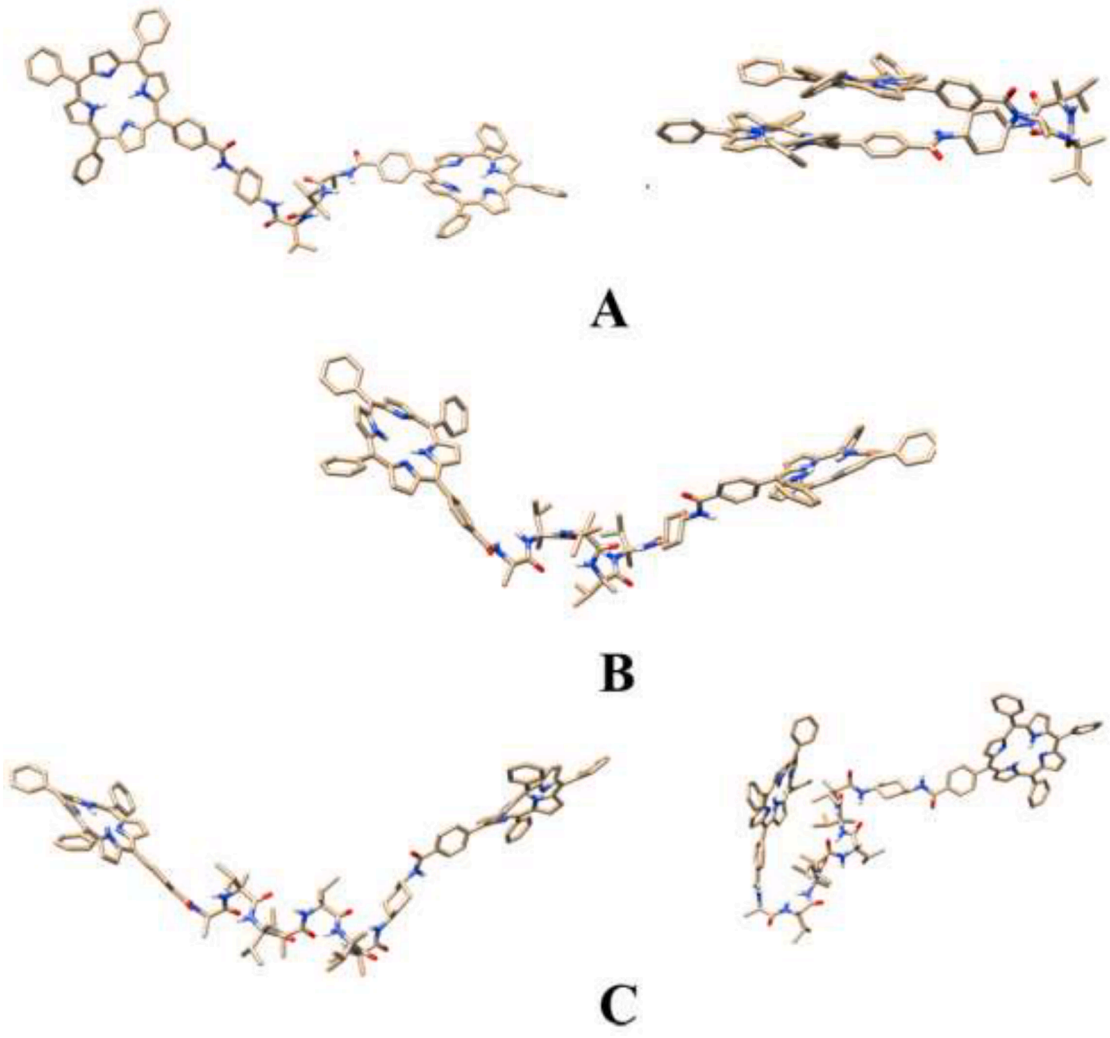

Fig. 5. Most representative structures of PMV2P (A), PMV4P (B) and PMV6P (C) as provided by cluster analysis of 200 ns MD simulations.

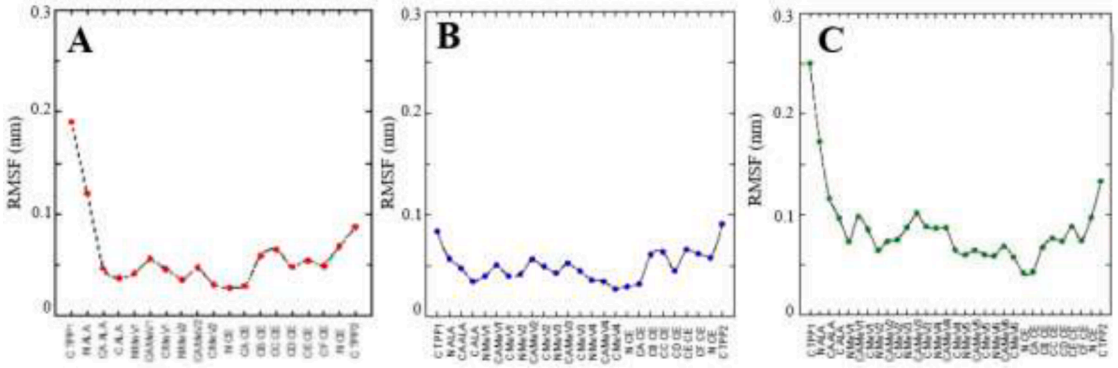

Fig. 6. RMSF of the components of the peptide chain linking the two porphyrin groups in PMV2P (A, red dots), PMV4P (B, blue dots) and PMV6P (C, green dots). The first and last entries of the abscissa refer to the C1 atoms of the two porphyrin groups.

cHe, connecting the N- and C-termini of the PMV4P peptide chain to the *bis*-porphyrin moieties, respectively (Fig. 6).

In the case of PMV4P, Ala(1) is involved in a peptide turn, stabilized by a HB between the TPP amide carbonyl group and the NH amide group of the N-terminal L-(αMe)Val (Scheme 1). This interaction was found only in the case of PMV4P. The cHe group also exhibits a limited mobility, which however is lower than that of the Ala-residues. As a result of the different mobility of the terminal linkers, the C1 atoms of the N-terminal TPP are characterized by a higher RMSF (2–2.5 Å) for PMV2P and PMV6P with respect to the RMSF obtained for the C1 atom of PMV4P (< 1 Å).

The conformational rigidity of the peptide bridge is confirmed by evaluating the distribution of the φ and ψ dihedral angles that, for all the L-(αMe)Val-residues, remain those typical of a 3_{10}-helical structure [16,

17]. The cHe torsional angles show a greater local mobility with respect to those of the L-(αMe)Val-residues, but, overall, also this moiety contributes to the conformational rigidity of the spacer. Most of the conformational flexibility of the *bis*-porphyrin peptide compounds investigated can therefore be ascribed to the dynamical properties of the Ala-residue, as shown by its C^{α} RMSF values and its dihedral angles fluctuations.

4. Conclusions

The photophysical properties of the *bis*-porphyrin fluorophores bridged by conformationally constrained peptide spacers have been investigated by steady-state and time-resolved spectroscopy techniques. MD simulations allowed to characterize the dynamical properties of the compounds, differing from each other by the length of the peptide bridge composed by two, four and six L-(αMe)Val-residues. Due to the rigidity of the peptide spacer, the two chromophores were located at a fixed distance and orientation, as confirmed by MD simulations. In the past, the porphyrin homodimers here investigated have been already studied by CD experiments, that revealed that the two fluorophores were coupled by chiral exciton interaction strongly dependent on the inter-chromophoric distance.

We showed that this interaction does not affect the singlet- and triplet-state properties of the porphyrin pair, nor its capacity to give rise to singlet-oxygen production. Interestingly, the singlet-oxygen quantum yield of the *bis*-porphyrin compounds investigated is lower than that of TPP, most likely because of steric and conformational effects. This conclusion is relevant due to the well-known properties of porphyrin compounds as photosensitizers for PDT therapy.

By femtosecond transient absorption it was possible to detect for the PMV*n*P compounds, but not for TPP, a characteristic decay time of some hundred picoseconds that we assigned to the decay of a trapped exciton species, associated to energy migration between the two symmetric chromophores [46]. The exciton migration is associated to the dynamics of the peptide chain: the more rigid the peptide chain, the slower the exciton time decay is. This conclusion is supported by the results of the MD simulations, that showed that the peptide spacer with four (αMe)Val-residues is the most rigid homologue of the series, due to a peculiar effect of the Ala-residue connecting the peptide chain to the porphyrin unit. The Ala-linker is rather mobile in PMV2P and PMV6P, but is almost rigid in PMV4P, because, in this case, it is conformationally constrained in the winding of a peptide turn.

The fluorescence anisotropy decays showed that due its rigid conformation, PMV4P features a higher rotation correlation time with respect to the more flexible PMV2P and PMV6P. However, femtosecond TAA of PMV4P in different viscosity environments, provides similar decay times, indicating that the formation of the related electronic states does not require a conformational rearrangement.

Summarizing the results discussed here, our *bis*-porphyrin system linked by an almost rigid peptide spacer shows photophysical properties almost similar to those of a single porphyrin chromophore from the nano- to the microsecond time scale, highlighting the weak nature of the porphryin-porphyrin interaction. Ultrafast time-resolved experiments reveal unique properties of these compounds, allowing to detect long-living transient species, that mediate the exciton coupling interaction between the two porphyrin groups. We judge these findings of relevance for the design of porphyrin-based chemicals for both PDT and DSSC applications.

Declaration of Competing Interest

The authors declare that they have no known competing financial interests or personal relationships that could have appeared to influence the work reported in this paper.

Acknowledgements

The research leading to the results of photophysical characterization in solution has received funding from the European Union's Horizon 2020 research and innovation program under grant agreement number 654148, Laserlab-Europe. MDZ gratefully acknowledges Centro Studi "Giorgio Levi Cases", Padua, Italy, for funding.

Supplementary materials

Supplementary material associated with this article can be found, in the online version, at doi:10.1016/j.jpap.2023.100191.

References

[1] J.M. Park, K.-I. Hong, H. Lee, W.-D. Jang, Bioinspired applications of porphyrin derivatives, Acc. Chem. Res. 54 (2021) 2249–2260, https://doi.org/10.1021/acs.accounts.1c00114.
[2] Y. Shi, F. Zhang, R.J. Linhardt, Porphyrin-based compounds and their applications in materials and medicine, Dyes and Pigments 188 (2021), 109136, https://doi.org/10.1016/j.dyepig.2021.109136.
[3] J. Kou, D. Dou, L. Yang, Porphyrin photosensitizers in photodynamic therapy and its applications, Oncotarget 8 (2017) 81591–81603, https://doi.org/10.18632/oncotarget.20189.
[4] K. Zeng, Z. Tong, L. Ma, W.-H. Zhu, W. Wu, Y. Xie, Molecular engineering strategies for fabricating efficient porphyrin-based dye-sensitized solar cells, Energy Environ. Sci. 13 (2020) 1617–1657, https://doi.org/10.1039/C)EE04200H.
[5] S. Ma, G. Verma, Porphyrin-Based Supramolecular Architectures. From Hierarchy to Functions, The Royal Society of Chemistry, London, 2022.
[6] J. Tian. B. Huang, M.H. Nawaz, W. Zhang, Recent advances of multidimensional porphyrin-based functional materials in photodynamic therapy, Coord. Chem. Rev. 420 (2020), 213410, https://doi.org/10.1016/j.ccr.2020.213410.
[7] B.M. Amos-Tautua, S.P. Songca, O.S. Oluwafemi, Application of porphyrins in antibacterial photodynamic therapy, Molecules 24 (2019) 2456, https://doi.org/10.3390/molecules24132456.
[8] C.L. Conway, I. Walker, A. Bell, D.J.H. Roberts, S.B. Brown, D.I. Vernon, *In vivo* and *in vitro* characterization of a protoporphyrin IX–cyclic RGD peptide conjugate for use in photodynamic therapy, Photochem. Photobiol. Sci. 7 (2008) 290–298, https://doi.org/10.1039/b715141a.
[9] S. Bettini, R. Pagano, V. Borovkov, G. Giancane, L. Valli, The role of the central metal ion of ethane-bridged bis-porphyrins in histidine sensing, J. Coll. Interf. Sci. 533 (2019) 762–770, https://doi.org/10.1016/j.jcis.2018.08.116.
[10] E.K. Yeow, P.J. Sintic, N.M. Cabral, J.N.H. Reek, M.J. Crossley, K.P. Ghiggino, Photoinduced energy and electron transfer in bis-porphyrins with quinoxaline Tröger's base and biquinoxalinyl spacers, Phys. Chem. Chem. Phys. 2 (2000) 4281–4291, https://doi.org/10.1039/B003612I.
[11] A.J.F.N. Sobral, S.M. Melo, M.L. Ramos, R. Teixeira, S.M. Andrade, S.M.B. Costa, Synthesis of flexible dimeric meso-tetrakis-porphyrins, Tetrahedron Lett 48 (2007) 3145–3149, https://doi.org/10.1016/j.tetlet.2007.03.047.
[12] D. Jokic, Z. Asfani, J. Weiss, The first versatile synthetic approach to cofacial bis-porphyrins with calixarene spacers, Org. Lett. 4 (2002) 2129–2132, https://doi.org/10.1021/ol0258583.
[13] W. Zhu, M. Sintic, Z. Ou, P.J. Sintic, J.A. McDonald, P.R. Brotherhood, M. J. Crossley, K.M. Kadish, Electrochemistry and spectroelectrochemistry of β,β′-fused quinoxalinoporphyrins and related extended bis-porphyrins with Co(III), Co(II), and Co(I) central metal ions, Inorg. Chem. 49 (2010) 1027–1038, https://doi.org/10.1021/ic901851u.
[14] S.I. Yang, R.K. Lammi, J. Seth, J.A. Riggs, T. Arai, D. Kim, D.F. Bocian, D. Holten, J. S. Lindsey, Excited-state energy transfer and ground-state hole/electron hopping in *p*-phenylene-linked porphyrin dimers, J. Phys. Chem. B 102 (1998) 9426–9436, https://doi.org/10.1021/jp982729o.
[15] B. Koszarna, H. Butenschön, D.T. Gryko, The synthesis and properties of bis-1,1′-(porphyrinyl)ferrocenes, Org. Biomol. Chem. 3 (2005) 2640–2645, https://doi.org/10.1039/B505366H.
[16] S. Oancea, F. Formaggio, S. Campestrini, Q.B. Broxterman, B. Kaptein, C. Toniolo, Distance dependency of exciton coupled circular dichroism using turn and helical peptide spacers, Biopolymers 72 (2003) 105–115, https://doi.org/10.1002/bip.10315.
[17] I. Guryanov, A. Moretto, S. Campestrini, Q.B. Broxterman, B. Kaptein, C. Peggion, F. Formaggio, C. Toniolo, Turn and helical peptide spacers: combined distance and angular dependencies in the exciton-coupled circular dichroism of intramolecularly interacting bis-porphyrins, Biopolymers 82 (2006) 482–490, https://doi.org/10.1002/bip.20500.
[18] B. Albinsson, J. Martensson, Excitation energy transfer in donor–bridge–acceptor systems, Phys. Chem. Chem. Phys. 12 (2010) 7338–8351, https://doi.org/10.1039/c003805a.
[19] B. Pispisa, A. Palleschi, L. Stella, M. Venanzi, C. Toniolo, A nitroxide derivative as a probe for conformational studies of short linear peptides in solution. Spectroscopic and molecular mechanics investigation, J. Phys. Chem. B 102 (1998) 7890–7898, https://doi.org/10.1021/jp981415y.
[20] B. Pispisa, C. Mazzuca, A. Palleschi, L. Stella, M. Venanzi, M. Wakselman, J.-P. Mazaylerat, M. Rainaldi, F. Formaggio, C. Toniolo, A combined spectroscopic

and theoretical study of a series of conformationally restricted hexapeptides carrying a rigid binaphthyl–nitroxide donor–acceptor pair, Chemistry. Eur. J. 17 (2003) 4084–4093, https://doi.org/10.1002/chem.200304727.
[21] A. Nakano, Y. Yasuda, T. Yamazaki, S. Akimoto, I. Yamazaki, H. Miyasaki, A. Itaya, M. Murakami, A. Osuka, Intramolecular energy transfer in S_1- and S_2-states of porphyrin trimers, J. Phys. Chem. A 105 (2001) 4822–4833, https://doi.org/10.1021/jp010596s.
[22] C.P. Gros, F. Brisach, A. Meristoudi, E. Espinosa, R. Guilard, P.D. Harvey, Modulation of the singlet−singlet through-space energy transfer rates in cofacial bisporphyrin and porphyrin−corrole dyads, Inorg. Chem. 46 (2017) 125–135, https://doi.org/10.1021/ic0613558.
[23] N.S. Hush, Distance dependence of electron transfer rates, Coord. Chem. Rev. 64 (1985) 135–157, https://doi.org/10.1016/0010-8545(85)80047-3.
[24] H.B. Gray, J.R. Winkler, Electron transfer through proteins, Q. Rev. Biophys. 36 (2003) 341–372, https://doi.org/10.1017/s0033583503003913.
[25] S.S. Isied, M.Y. Ogawa, J.F. Wishart, Peptide-mediated intramolecular electron transfer: long-range distance dependence, Chem. Rev. 92 (1992) 381–394, https://doi.org/10.1021/cr00011a002.
[26] R.A. Malak, Z. Gao, J.F. Wishart, S.S. Isied, Long-range electron transfer across peptide bridges: the transition from electron superexchange to hopping, J. Am. Chem. Soc. 126 (2004) 13888–13889, https://doi.org/10.1021/ja0401040.
[27] E. Gatto, L. Stella, C. Baldini, C. Toniolo, F. Formaggio, M. Crisma, M. Venanzi, Photocurrent generation through peptide-based self-assembled monolayers formed by functionalized conformationally constrained peptides on gold electrodes, J. Pept. Sci. 46 (2018) 184–191, https://doi.org/10.1002/psc.1329.
[28] M. Venanzi, E. Gatto, M. Caruso, A. Porchetta, F. Formaggio, C. Toniolo, Photoinduced electron transfer through peptide-based self-assembled monolayers chemisorbed on gold electrodes: directing the flow-in and flow-out of electrons through peptide helices, J. Phys. Chem. A 118 (2118) (2014) 6674–6684, https://doi.org/10.1021/jp503791wù.
[29] E. Gatto, A. Quatela, M. Caruso, R. Tagliaferro, M. De Zotti, F. Formaggio, C. Toniolo, A. Di Carlo, M. Venanzi, Mimicking nature: a novel peptide-based bio-inspired approach for solar energy conversion, ChemPhysChem 15 (2014) 64–68, https://doi.org/10.1002/cphc.201300901.
[30] C. Toniolo, M. Crisma, F. Formaggio, C. Peggion, Control of peptide conformation by the Thorpe-Ingold effect(C^{α}-tetrasubstitution), Biopolymers (Pept. Sci.) 60 (2001) 396–419, https://doi.org/10.1002/1097-0282(2001)60:6%3C396::AID-BIP10184%3E3.0.CO;2-7.
[31] E. Gatto, A. Porchetta, L. Stella, I. Guryanov, F. Formaggio, C. Toniolo, B. Kaptein, Q.B. Broxterman, M. Venanzi, Conformational effects on the electron transfer efficiency in peptide foldamers based on α,α-disubstituted glycyl residues, Chem. Biodivers 5 (2008) 1263–1278, https://doi.org/10.1002/cbdv.200890113.
[32] B. Pispisa, C. Mazzuca, A. Palleschi, L. Stella, M. Venanzi, F. Formaggio, A. Polese, C. Toniolo, Structural features of linear (αMe)Val-based peptides in solution by photophysical and theoretical conformational studies, Biopolym. (Pept. Sci.) 55 (2000) 425–435, https://doi.org/10.1002/1097-0282(2000)55:6%3C425::AID-BIP1018%3E3.0.CO;2-K.
[33] S. Mammi, M. Rainaldi, M. Bellanda, E. Schievano, E. Peggion, Q.B. Broxterman, F. Formaggio, M. Crisma, C. Toniolo, Concomitant occurrence of peptide 3_{10}- and α-helices probed by NMR, J. Am. Chem. Soc. 122 (2000) 11735–11736, https://doi.org/10.1021/ja002710a.
[34] K.A. Bolin, G.L. Millhauser, α and 3_{10}: the split personality of polypeptide helices, Acc. Chem. Res. 32 (1999) 1027–1033, https://doi.org/10.1021/ar980065v.
[35] A.M. Brouwer, Standards for photoluminescence quantum yield measurements in solution (IUPAC Technical Report), Pure Appl. Chem. 83 (2011) 2213–2228, https://doi.org/10.1351/PAC-REP-12-03-03.
[36] G. Stricker, V. Subramaniam, C.A.M. Seidel, A. Volkmer, Photochromicity and fluorescence lifetimes of green fluorescent proteins, J. Phys. Chem. B 103 (1999) 8612–8617, https://doi.org/10.1021/jp991425e.
[37] H.J.C. Berendsen, D. van der Spoel, R. van Drunen, GROMACS: a message-passing parallel molecular dynamics implementation, Comp. Phys. Comm. 91 (1995) 43–56, https://doi.org/10.1016/0010-4655(95)00042-E.
[38] P.M.R. Paulo, J.N. Canongia Lopes, S.M.B. Costa, Molecular dynamics simulations of porphyrin-dendrimer systems: toward modeling electron transfer in solution, J. Phys. Chem. B 112 (2008) 14779–14792, https://doi.org/10.1021/jp806849y.
[39] X. Grabuleda, C. Jaime, P.A. Kollman, Molecular dynamics simulation studies of liquid acetonitrile: new six-site model, J. Comput. Chem. 21 (2000) 901–908, https://doi.org/10.1002/1096-987X(20000730)21:10%3C901::AID-JCC7%3E3.0.CO;2-F.
[40] A.Credi M. Montalti, L. Prodi, M.T. Gandolfi, Handbook of Photochemistry, 3rd Ed, CRC Press, 2006, https://doi.org/10.1201/9781420015195.
[41] J. Seixas de Melo, A.P. Moura, M.J. Melo, Photophysical and spectroscopic studies of indigo derivatives in their keto and leuco forms, J. Phys. Chem. A 108 (2004) 6975–6981, https://doi.org/10.1021/jp049076y.
[42] R. Schmidt, C. Tanielian, R. Dunsbach, Wolff C, Phenalenone, a universal reference compound for the determination of quantum yields of singlet oxygen $O_2(^1\Delta_g)$ sensitization, J. Photochem. Photobiol. A: Chem. 79 (1994) 11–17, https://doi.org/10.1016/1010-6030(93)03746-4.
[43] W. Wilkinson, W.P. Helman, A.B. Ross, Quantum yields for the photosensitized formation of the lowest electronically excited singlet state of molecular oxygen in solution, J. Phys. Chem. Reference Data 22 (1993) 113–262, https://doi.org/10.1063/1.555934.
[44] J.S. Baskin, H.-Z. Yu, A.H. Zewail, Ultrafast dynamics of porphyrins in the condensed phase: I. Free base tetraphenylporphyrin, J. Phys. Chem. A 106 (2002) 9837–9844, https://doi.org/10.1021/jp020398g.
[45] M. Fujitsuka, M. Hara, S. Tojo, A. Okada, V. Troiani, N. Solladié, T. Majima, Fast exciton migration in porphyrin-functionalized polypeptides, J. Phys. Chem. Lett. B 109 (2005) 33–35, https://doi.org/10.1021/jp044866t.
[46] O.F. Dimitriev, Dynamics of excitons in conjugated molecules and organic semiconductor systems, Chem. Rev. 122 (2022) 8487–8593, https://doi.org/10.1021/acs.chemrev.1c00648.